International Journal of Applied Engineering Research ISSN 0973-4562 Volume 13, Number 12 (2018) pp. 10991-11000
© Research India Publications. http://www.ripublication.com

Effect Of Magnetic Field And Radiation On MHD Heat And Mass Transfer Of Micropolar Fluid Over Stretching Sheet With Soret And Dufour Effects.

S.R. RaviChandra babu[a*]

[a]*Research scholar, Department of mathematics, JNTUA, Anantapur, A.P, India.*

S. Venkateswarlu[b]

[b]*Department of mathematics, RGM College of Engineering & Technology, Nandyal, A.P, India.*

K. Jaya Lakshmi[c]

[c]*Department of mathematics, JNTUA, Anantapur, A.P, India.*

Corresponding author

Abstract

The influence of magnetic field and radiation on unsteady MHD boundary layer flow, heat and mass transfer analysis over a stretching sheet embedded in porous media filled with viscous micropolar fluid is numerically investigated. The governing conservation equations are converted into the set of ordinary differential equations and are solved numerically by using Finite element method. The influence of key non-dimensional parameters, namely, suction parameter, Magnetic parameter, Unsteadiness parameter, Eckert number, Soret parameter, Dufour parameter and Micro-rotation parameter on velocity, micro-rotation, temperature and concentration profiles are portrayed graphically. Furthermore, skin-friction coefficient, couple stress coefficient, rates of heat and mass transfer for various values of the governing parameters are calculated and the results are summarized in tabular form.

Keywords: MHD, Thermal Radiation, Micropolar fluid, Soret effect, Dufour effect, Finite element method.

INTRODUCTION

Micropolar fluids has been an active area of research for several decades, because of its wide range of applications in analyzing fluid flow in brain, exotic lubricants, liquid crystals, blood flow in animals, etc. In this theory, the continuum is regarded as sets of structured particles which contain not only mass and velocity, but also a substructure. That is, each material volume element contains micro volume elements that can translate and rotate independently of the motion of micro volume. In this model, two independent kinematic vector fields are introduced – one representing the translation velocities of fluid particles; and the other representing angular (spin) velocities of the particles, called as microrotation vector. The theory of micropolar fluids was originally formulated by Eringen (1999) by taking the local effects arising from the microstructure and the intrinsic motion of the fluid into the account. The more detail of this theory and its applications can be found in Ariman et al. (1974) and books by Lukaszewicz (1999) and Eringen (2001). Chamkha et al. (2011) has presented the impact of Joule heating, radiation and chemical reaction on unsteady MHD micropolar fluid past a heated vertical plate. Rahman et al. (2009) described heat and mass transfer flow of micropolar fluid over inclined vertical plate under the influence of variable thermal conductivity, non – uniform heat source/sink and surface heat flux. El-Amin et al. (2001) have analyzed the influence of suction on flow and mass transfer analysis of micropolar fluid over vertical plate by taking magnetic field into the account. Rashidi et al. (2011) have presented the effect of radiation on heat transfer flow of micropolar fluid saturated in porous media and Homotopy analysis method (HAM) is used to obtain accurate and analytical solution. Shadloo et al. (2013) discussed the heat transfer flow of micropolar fluid over stretching sheet embedded in porous media with thermal radiation. Bhargava et al. (2003) have presented heat and mass transfer characteristics of micropolar fluid over porous stretching sheet with suction/injection. Ibrahim et al. (2008) analyzed unsteady MHD mixed convection flow of a micropolar fluid by taking viscous dissipation and thermal radiation into the account. Damseh Rebhi et al. (2009) have perceived the influence of heat generation/absorption and first-order chemical reaction on micropolar fluid flow over a uniform stretching sheet. Yacob et al. (2011) have reported boundary layer heat transfer stagnation-point flow of micropolar fluid over a stretching/shrinking sheet and presented dual solution for shrinking case and unique solution for stretching case. Rosali et al. (2012) analyzed micropolar fluid flow through porous media over a stretching/shrinking sheet with suction. Mahmood et al. (2013) have perceived steady stagnation point flow, heat transfer analysis of micropolar second grade fluid over a stretching sheet. They found that fluid velocity remarkably enhances with higher values of micro – rotation parameter. Pal et al. (2015) deliberated the impact of non – uniform heat source/sink on Darcy–Forchheimer convective flow of micro – polar fluid over stretching sheet with radiation.

The applications of Soret and Dufour effects can be found in the area of reactor safety, combustion flames and solar collectors as well as building energy conservation In view of above applications several others (Dulal Pal and Mondal 2011, Makinde 2011, Reddy and Rao 2012, Chamkha and

Rashad 2014, Sudarsana Reddy and Chamkha 2016c) have discussed the impact of Soret and Dufour effects on boundary layer heat and mass transfer flow over different geometries. Wang (2004) was first studied the unsteady boundary layer flow of a liquid film over a stretching sheet. Ishak (2010) has presented unsteady MHD flow and heat transfer behavior over a stretching plate. Recently, Dulal pal (2011) has described the analysis of flow and heat transfer over an unsteady stretching surface with non-uniform heat source/sink and thermal radiation. Sarma et al. (2015) perceived the influence of magnetic field and thermal radiation on mixed convective flow over a vertical plate embedded in porous media with chemical reaction. Mishra et al. (2016) discussed the boundary layer flow over a stretching cylinder with velocity slip and thermal jump.

MATHEMATICAL ANALYSIS

We consider two-dimensional, unsteady, viscous, electrically conducting, heat and mass transfer of micropolar fluid flow through porous medium over a stretching sheet in the presence of suction/injection, Soret and Dufour effects. The coordinate system is such that x-axis is taken along the stretching surface in the direction of the motion with the slot at origin, and the y-axis is perpendicular to the surface of the sheet as shown schematically in Fig. 1. A uniform transverse magnetic field (B_0) is applied along the y-axis. The stretching surface and the fluid are maintained same temperature and concentration initially, instantaneously they raised to a temperature $T_w(> T_\infty)$ and concentration $C_w(> C_\infty)$ which remain unchanged. Under the above stated physical situations and the reference works of Mohanty et al. (2015), the governing boundary-layer and Darcy-Boussinesq's approximations the basic equations are given by:

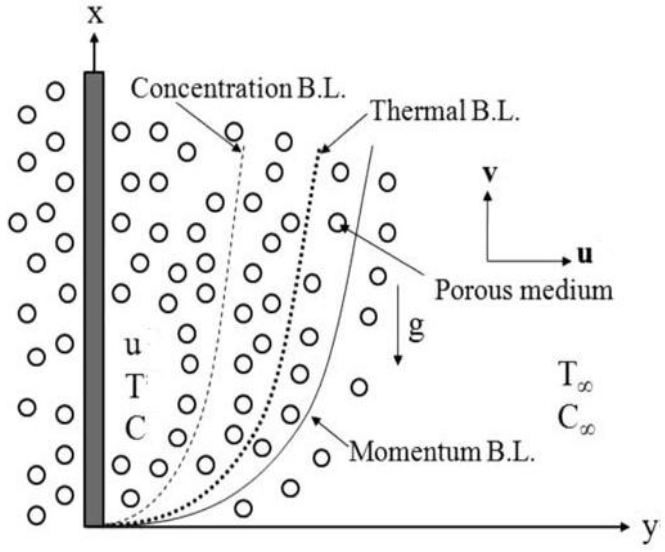

Figure 1. Mathematical model of the problem.

$$\frac{\partial u}{\partial x}+\frac{\partial v}{\partial y}=0 \tag{1}$$

$$\frac{\partial u}{\partial t}+u\frac{\partial u}{\partial x}+v\frac{\partial u}{\partial y}=\left(\frac{\mu+\kappa}{\rho}\right)\frac{\partial^2 u}{\partial y^2}+\left(\frac{\kappa}{\rho}\right)\frac{\partial W}{\partial y}+ g_a[\beta(T-T_\infty)+\beta'(C-C_\infty)]-\frac{\mu}{\rho\kappa}u-\frac{\sigma B_0^2}{\rho}u \tag{2}$$

$$\frac{\partial W}{\partial t}+u\frac{\partial W}{\partial x}+v\frac{\partial W}{\partial y}=-\frac{\kappa}{\rho J}\left(2W+\frac{\partial u}{\partial y}\right)+\frac{\gamma}{\rho J}\frac{\partial^2 W}{\partial y^2} \tag{3}$$

$$\frac{\partial T}{\partial t}+u\frac{\partial T}{\partial x}+v\frac{\partial T}{\partial y}=\alpha\frac{\partial^2 T}{\partial y^2}+\frac{\nu}{c_p}\left(\frac{\partial u}{\partial y}\right)^2+\frac{D_m k_T}{c_s c_p}\frac{\partial^2 C}{\partial y^2}-\frac{1}{\rho c_p}\frac{\partial q_r}{\partial y} \tag{4}$$

$$\frac{\partial C}{\partial t}+u\frac{\partial C}{\partial x}+v\frac{\partial C}{\partial y}=D_m\frac{\partial^2 C}{\partial y^2}+\frac{D_m k_T}{T_m}\frac{\partial^2 T}{\partial y^2} \tag{5}$$

The associated boundary conditions on the vertical surface are defined as follows,

$$u=U_w(x)=ax,\ v=V_1(x),\ T=T_w,\ C=C_w,\quad W=0,\quad at\ y=0.$$
$$u\to 0,\ W\to 0,\ T\to T_\infty, C\to C_\infty,\quad at\ y\to\infty. \tag{6}$$

The term $V_1=-\sqrt{\frac{va}{2}}V_0$ represents the mass transfer at the surface with $V_1<0$ for suction and $V_1>0$ for injection.

By using Rosseland approximation for radiation, the radiative heat flux q_r is defined as

$$q_r=-\frac{4\sigma^*}{3K^*}\frac{\partial T^4}{\partial y} \tag{7}$$

where, σ^* is the Stephan-Boltzman constant, K^* is the mean absorption coefficient. We assume that the temperature differences within the flow are such that the term T^4 may be expressed as a linear function of temperature. This is accomplished by expanding T^4 in a Taylor series about the free stream temperature T_∞ as follows:

$$T^4={T_\infty}^4+4{T_\infty}^3(T-T_\infty)+6{T_\infty}^2(T-T_\infty)^2+\cdots \tag{8}$$

Neglecting higher-order terms in the above equation (12) beyond the first degree in $(T-T_\infty)$, we get

$$T^4\cong 4{T_\infty}^3T-3{T_\infty}^4 \tag{9}$$

.

Thus, substituting Eq. (9) into Eq. (7), we get

$$q_r=-\frac{16{T_\infty}^3\sigma^*}{3K^*}\frac{\partial T}{\partial y}. \tag{10}$$

The following similarity transformations are introduced to simplify the mathematical analysis of the problem

$$\eta = \sqrt{\frac{a}{\nu(1-ct)}}\, y,\ \psi = \sqrt{\frac{\nu a}{1-ct}}\, f,\ u = \frac{ax}{1-ct} f'$$

$$v = -\sqrt{\frac{\nu a}{1-ct}}\, f,\ W = \sqrt{\frac{a^3}{\nu(1-ct)^3}}\, x\, g$$

$$T = T_\infty + \frac{bx}{(1-ct)^2}\theta\ ,\ C = C_\infty + \frac{dx}{(1-ct)^2}\,\phi. \tag{11}$$

Using eqn. (7), the governing equations (2) – (5) are transformed into the following form

$$(1+A1)f''' + ff'' - f'^2 - A\left(f' + \frac{1}{2}\eta\, f''\right) + A1g' + g_r\theta + g_m\phi - (M+K)\, f' = 0 \tag{12}$$

$$\lambda g'' + fg' - gf' - \frac{A}{2}(3g + \eta\, g') + A1\, B(2g + f'') = 0 \tag{13}$$

$$\theta'' + Pr(\, f\, \theta' - f'\theta) - Pr\ \frac{A}{2}\ (4\theta + \eta\, \theta') + Ec\ (f'')^2 + Du\ \phi'' = 0 \tag{14}$$

$$\phi'' - Sc\ (\, f'\phi - \ f\ \phi') - Sc\ \ \frac{A}{2}\ (4\phi + \eta\ \phi') + Sc\ Sr\ \theta'' = 0 \tag{15}$$

The corresponding transformed boundary conditions are

$$f' = 1, f = V_0, g = 0, \theta = 1, \phi = 1,\ \text{at}\quad y = 0$$

$$f' = 0,\ g = 0,\quad \theta = 0,\ \phi = 0\quad \text{at}\quad y \to \infty \tag{16}$$

Where $A1 = \frac{\kappa}{\mu}$, $g_r = \frac{g_a \beta b}{a^2}$, $g_m = \frac{g_a \beta' l}{a^2}$, $A = \frac{c}{a}$

$$K = \frac{\nu(1-ct)}{k\, a},\quad Pr = \frac{\nu}{\alpha},\ \lambda_0 = \frac{\nu}{\mu\, j}$$

$$Sc = \frac{\nu}{D_m},\ B = \frac{\nu\,(1-ct)}{j\, a},\ Du = \frac{D_m k_T\, l}{c_s c_p b\, \nu}$$

$$Sr = \frac{D_m k_T}{\nu T_m},\quad Ec = \frac{a^2 x}{c_p\, b},\quad M = \frac{\sigma B_0^2 (1-ct)}{\rho\, a}.$$

The major physical quantities of interest in this problem are the local skin friction coefficient (C_{fx}), couple stress coefficient (C_{sx}), local Nusselt number (Nu_x) and the local Sherwood number (Sh_x) are defined, respectively, by

$$C_{fx} = \frac{2(1+A1)\, f''(0)}{Re_x^{\frac{1}{2}}},\ C_{sx} = \frac{\nu\, a\, U_w h'(0)}{Re_x^{\frac{1}{2}}},$$

$$Nu_x = -\frac{\theta'(0)}{Re_x^{\frac{1}{2}}}\ ,\quad Sh_x = -\frac{\phi'(0)}{Re_x^{\frac{1}{2}}}.$$

NUMERICAL METHOD OF SOLUTION

The set of ordinary differential equations (12) – (15) are highly non-linear, and therefore cannot be solved analytically. The Finite-element method (Sudarsana Reddy et al. 2016a, 2016b, Rana et al. 2012) has been employed to solve these non-linear equations. The procedure of Finite element method is as follows.

(i) Finite-element discretization

(ii) Generation of the element equations

(iii) Assembly of element equations

(iv) Imposition of boundary conditions

(v) Solution of assembled equations

RESULTS AND DISCUSSION

The numerical solution of Eqns. (12) – (15) is presented by means of Finite element method and the results are presented in Figs. 2 – 21. The validation of the current numerical method is performed with the results obtained by Mohanty et al. [36] and is shown in Table 1.

Figures 2 – 5 illustrates the velocity, micro-rotation, temperature and concentration profiles for various values of suction/injection parameter (V_0). It is observed from fig.2 that the velocity of the fluid decreases with increase in the value of the suction parameter ($V_0 > 0$). The micro-rotation profiles also decelerates with increasing values of ($V_0 > 0$). It is seen observed that temperature profiles decreases with increase in the values of ($V_0 > 0$). This is due to the fact that the presence of wall suction has the tendency to reduce the thermal boundary layer thickness which results the reduction in the temperature profiles (Fig. 4). Furthermore, the concentration profiles also diminishes in the boundary layer regime with increase in the values of ($V_0 > 0$).

The influence of magnetic field parameter (M) on velocity, micro-rotation and temperature profiles in the boundary layer regime is depicted in Figs. 6 - 8. It is noticed from these figures that the hydrodynamic and micro-rotation boundary layer thickness depreciates (Figs. 6 & 7), whereas, thermal boundary layer thickness enhances (Fig. 8) with the higher values of (M). The impact of thermal Grashof number (G_r) on velocity distributions is depicted in Fig. 9 and found that the hydrodynamic boundary layer thickness elevates with rising values of (G_r).

The fluid velocity is increasing function of mass Grashof number (G_m) as shown in Fig. 10. The influence of unsteadiness parameter (τ) on temperature and concentration profiles is depicted in figures 11 – 12. It can be seen that

temperature profiles decelerates with increase in the values of unsteadiness parameter (τ) as shown in Fig. 11. Furthermore, the concentration profiles also decreases in the flow region and is shown in Fig. 12.

Figure 13 depicts the effect of Eckert number (*Ec*) on temperature profiles in the boundary layer regime. The thickness of thermal boundary layer is boosted in the flow region as the values of Eckert number (*Ec*) rises. The sway of thermal radiation parameter (*R*) on temperature and concentration profiles is portrayed in Figs. 14 – 15. We noticed from these figures that the thermal boundary layer thickness elevates, whereas, solutal boundary layer thickness diminishes with rising values of (*R*).

The impact of Soret effect (*Sr*) on temperature and concentration profiles is portrayed in Figs. 16 – 17. It is clearly observed that the temperature distributions decrease, however, concentration profiles increases at all points in the flow field with the increasing values of Soret number (*Sr*). This is because of the fact that the diffusive species with higher values of Soret parameter (*Sr*) has the tendency of increasing concentration profiles.

The impact of Dufour number (*Du*) on temperature and concentration profiles is portrayed in Figs. 18 – 19. The temperature of the fluid raises, however, the concentration of the fluid decelerates in the boundary layer regime as the (*Du*) increases. The velocity and micro-rotation distributions for diverse values of micropolar parameter (*A1*) in the boundary layer regime is scattered from Figs. 20 – 21. It is worth to mention that both profiles heighten in the fluid regime with the increasing values of (*A1*). This is because of the fact that higher the values of (*A1*) has the tendency of increasing the thickness of both momentum and micro-rotation boundary layers.

The variation in the values of local skin-friction co-efficient $(f''(0))$, couple stress coefficient$(h'(0))$, local Nusselt number $(-\theta'(0))$ and local Sherwood number $(-\phi'(0))$ for different values of governing parameters is presented in Table 2. It is seen from table that the values of local skin-friction co-efficient, Nusselt number and Sherwood numbers are depreciates, whereas, the values of couple stress coefficient elevates with increase in the values of (*M*). It is clear from this table that the values of skin-friction coefficient worsens, however, the couple stress coefficient, dimensionless heat and mass transfer rates are boosted with the higher values of suction parameter ($V_0 > 0$). It is clear from this table that the values of skin-friction coefficient and Sherwood number are increased, whereas, the values of micro-rotation and Nusselt number diminishes with the higher values of (*R*). It is noticed that the values of $(f''(0))$, $(h'(0))$ and $(-\phi'(0))$ decreases, whereas, $(-\theta'(0))$ values hightens as the values of (*Sr*) rises. The dimensionless velocity, micro-rotation and heat transfer rates are decreased, whereas, the dimensionless mass transfer rates increases with the increasing values of (*Du*). The values of all non-dimensional parameters, skin-friction co-efficient, couple stress coefficient, local Nusselt number and Sherwood number upsurges as the values of micro-rotation parameter (*A1*) increases.

CONCLUSION

The combined influence of Thermo – diffusion and Diffusion – thermo effect on unsteady MHD boundary layer flow, heat and mass transfer characteristics of viscous micropolar fluid over a stretching sheet by taking suction/injection into the account is studied numerically in this paper. The important findings of this study are summarized as follows: Suction parameter ($V_0 > 0$) deteriorates the velocity, angular velocity, temperature and concentration of the fluid in the boundary layer regime. The velocity of the fluid diminishes, whereas, temperature of the fluid heightens with rising values of (*M*) and is because of the fact that the presence of magnetic field into the flow produces Lorentz force, which resist the motion of the fluid causes enhancement in the temperature. Soret effect enhances the concentration profiles, whereas, depreciates the temperature profiles. However, exact reverse trend is noticed in the profiles with higher values of (*Du*).

REFERENCES

[1]. Ariman, T. Turk, M.A. and Sylvester, N.D., (1974) Application of micro continuum fluid Mechanics, *Int. J. Eng. Sci.,* 12, pp. 273-293.

[2]. Bhargava, R. Kumar, L. and Takhar, H.S., (2003) Finite element solution of mixed convection micropolar fluid driven by a porous stretching sheet, *Int. J. Eng. Sci.,* 41, pp. 2161–2178.

[3]. Chamkha, A.J. and Rashad, A.M., (2014) Unsteady heat and mass transfer by MHD mixed convection flow from a rotating vertical cone with chemical reaction and Soret and Dufour effects, *The Canadian Journal of Chemical Engineering, DOI 10.1002/cjce.21894*.

[4]. Chamkha, A. J. Mohammad, R.A. and Ahmad, E., (2011) Unsteady MHD natural convection from a heated vertical porous plate in a micropolar fluid with Joule heating, chemical reaction and radiation effects, *Meccanica,* 46, pp. 399 – 411.

[5]. Damseh Rebhi, A. Al-Odat, M.Q. Chamkha, Ali.J. and Shannak Benbella, A., (2009), Combined effect of heat generation or absorption and first-order chemical reaction on micropolar fluid flows over a uniformly stretched permeable surface, *Int. J. Therm. Sci.,* 48, pp. 1658–1663.

[6]. Dulal Pal. and Mondal, H., (2011) MHD non-Darcian mixed convection heat and mass transfer over a non-linear stretching sheet with Soret and Dufour effects and chemical reaction, *International communications in heat and mass transfer,* pp. 463-467.

[7]. Dulal pal., (2011) Combined effects of non-uniform heat source/sink and thermal radiation on heat transfer over an unsteady stretching permeable surface, *Commun Nonlinear Sci Numer. Simulat.,* 16, pp. 1890–1904.

[8]. El-Amin, M.F., (2001) Magneto hydrodynamic free convection and mass transfer flow in micropolar fluid with constant suction, *J. Mag. Mag. Mater.,* 234, pp. 567–574.

[9]. Eringen, A.C., (1996) Theory of micropolar fluids, *J. Math. Mech.,* 16, pp. 1-18.

[10]. Eringen, A.C., (2001) Micro continuum field theories II, fluent media, *Springer,* New York.

[11]. Ibrahim, F.S. Elaiw, A.M. and Bakr, A.A., (2008) Influence of viscous dissipation and radiation on unsteady MHD mixed convection flow of micropolar fluids, *Appl. Math. Inf. Sci.,* 2, pp. 143–162.

[12]. Ishak, A., (2010) Unsteady MHD flow and heat transfer over a stretching plate, *J. Applied Sci.,* 10, pp. 2127-2131.

[13]. Lukaszewicz, G., (1999) Micropolar fluids: theory and application. *Birkhäuser Basel*.

[14]. Mahmood, R. Nadeem, S. and Akber, N.S., (2013) Non-orthogonal stagnation point flow of a micropolar second grade fluid towards a stretching surface with heat transfer, *J. Taiwan Inst. Chem. Eng.,*44, pp. 586–595.

[15]. Makinde, O.D., (2011) On MHD mixed convection with Soret and Dufour effects past a vertical plate embedded in a porous medium, *Latin American Applied Research* 41, pp. 63-68.

[16]. Mishra, U. Gurminder Singh., (2016) A study of mixed convection flow over stretching cylinder in presence of slip flow and thermal jump boundary conditions, *International Journal of Fluid Mechanics Research* 43, pp. 308-318.

[17]. Mohanty, B. Mishra, S.R. and Pattanayak, H.B., (2015) Numerical investigation on heat and mass transfer effect of micropolar fluid over a stretching sheet through porous media, *Alexandria Engineering Journal* 54, pp. 223–232.

[18]. Pal, D. and Chatterjee, S., (2015) Effects of radiation on Darcy–Forchheimer convective flow over a stretching sheet in a micropolar fluid with non-uniform heat source/sink, *J. Appl. Fluid Mech.,* 8, 207–212.

[19]. Rahman, M. M. Uddin, M.J. and Aziz, A., (2009) Effects of variable electric conductivity and non-uniform heat source (or sink) on convective micropolar fluid flow along an inclined flat plate with surface heat flux. *Int. J. Ther. Sci.,* 48, pp. 2331–2340.

[20]. Rana, P. and Bhargava, R., (2012) Flow and heat transfer of a nanofluid over a nonlinearly stretching sheet: a numerical study, *Comm. Nonlinear Sci. Numer. Simulat.,*17, pp. 212 – 226.

[21]. Rashidi, M.M. Mohimanian pour, S.A. and Abbasbandy,S., (2011) Analytic approximate solutions for heat transfer of a micropolar fluid through a porous medium with radiation, *Commun. Nonlinear Sci. Numer. Simul.,* 16, pp. 1874–1889.

[22]. Reddy, P.S. and Rao, V.P., (2012) Thermo-Diffusion and Diffusion –Thermo Effects on convective heat and mass transfer through a porous medium in a circular cylindrical annulus with quadratic density temperature variation – Finite element study. *Journal of Applied Fluid Mechanics,* 5(4), pp. 139-144.

[23]. Rosali, H. Ishak, A. and Pop. I., (2012) Micropolar fluid flow towards a stretching/shrinking sheet in a porous medium with suction, *Int. Commun. Heat MassTransf.* 39, pp. 826–829.

[24]. Sarma, D. Kamalesh K. Pandit., (2015) Effects of thermal radiation and chemical reaction on steady mhd mixed convective flow over a vertical porous plate with induced magnetic field, *International Journal of Fluid Mechanics Research* 42, pp. 315-333.

[25]. Shadloo, M.S. Kimiaeifar, A. and Bagheri D., (2013) Series solution for heat transfer of continues stretching sheet immersed in a micropolar fluid in the existence of radiation, *Int. J. Numer. Meth. Heat Fluid Flow* 23, pp. 289–304.

[26]. Sudarsana Reddy, P. and Chamkha, A.J., (2016a) Soret and Dufour effects on MHD heat and mass ransfer flow of a micropolar fluid with thermophoresis particle deposition, *Journal of Naval Architechure and Marine Engineering* 13, pp. 39-50.

[27]. Sudarsana Reddy, P. and Chamkha, A.J., (2016b) Soret and Dufour effects on unsteady mhd heat and mass transfer over a stretching sheet with thermophoresis and non-uniform heat generation/absorption, *Journal of Applied Fluid Mechanics* 9, pp. 2443-2455.

[28]. Sudarsana Reddy, P. and Chamkha, A.J., (2016c), Soret and Dufour effects on MHD convective flow of Al_2O_3–water and TiO_2–water nanofluids past a stretching sheet in porous media with heat generation/absorption, *Advanced Powder Technology* 27, pp. 1207-1218.

[29]. Yacob, N.A. Ishak, A. and Pop. I., (2011) Melting heat transfer in boundary layer Stagnation – point flow towards a stretching/shrinking sheet in a micropolar fluid, *Comput.Fluids* 47, pp. 16–21.

Table 1: Comparison of local Skin-friction, Nusselt number and Sherwood number with the existing results, when $Sr = 0, Du = 0, \mathrm{G1} = 0.5, Vo = 0, B1 = 0.1, \tau = 0, \lambda = 0.5.$

Parameter							C_f		Nu_x		Sh_x	
Gr	Gc	Pr	Sc	M	K	Ec	Mohanty et al. [2015]	Present Study	Mohanty et al. [2015]	Present Study	Mohanty et al. [2015]	Present Study
0.0	0.0	0.72	0.00	0	100	0.00	-0.81861	-0.81873	0.85604	0.85619	0.16666	0.16671
0.1	0.0	0.72	0.00	0	100	0.00	-0.78025	-0.78019	0.86514	0.86526	0.42252	0.42263
0.1	0.0	0.72	0.22	0	100	0.00	-0.78025	-0.78019	0.86514	0.86526	0.42252	0.42263
0.1	0.0	0.72	0.22	1	100	0.00	-1.11781	-1.11776	0.78477	0.78482	0.37866	0.37872
0.1	0.0	0.72	0.22	1	0.5	0.01	-1.59782	-1.59773	0.68391	0.68386	0.33393	0.33385
0.1	0.0	0.72	0.22	1	100	0.01	-1.11775	-1.11766	0.77999	0.77981	0.37867	0.37874
0.1	0.0	0.72	0.22	1	0.5	0.01	-1.59777	-1.59782	0.67651	0.67646	0.33394	0.33398
0.1	0.1	7.00	0.22	1	100	0.01	-1.09307	-1.09311	3.02046	3.02052	0.38361	0.38370
0.5	0.1	0.72	0.22	1	100	0.01	-0.93986	-0.93991	0.82922	0.82931	0.40495	0.40486
0.1	0.1	0.72	0.22	1	100	0.01	-1.06792	-1.06798	0.79858	0.79863	0.38891	0.38896
0.5	0.1	0.72	0.22	1	0.5	0.01	-1.44651	-1.44667	0.72576	0.72569	0.35583	0.35591

Table 2: Influence of various parameters on Skin-friction co-efficient $(f''(0))$, Couple stress coefficient $(h'(0))$, local Nusselt number $(-\theta'(0))$ and local Sherwood number $(-\phi'(0))$ with fixed values of other parameters.

M	V_0	R	Sr	Du	$A1$	C_{fx}	C_{sx}	Nu_x	Sh_x
0.1	0.5	0.5	1.0	0.1	0.1	−0.029503	0.020189	1.263071	0.930092
0.4	0.5	0.5	1.0	0.1	0.1	−0.140078	0.023735	1.247951	0.916867
0.7	0.5	0.5	1.0	0.1	0.1	−0.334706	0.027632	1.230871	0.902205
1.0	0.5	0.5	1.0	0.1	0.1	−0.513352	0.031039	1.215510	0.889266
1.5	0.5	0.5	1.0	0.1	0.1	−0.678789	0.034055	1.201602	0.877778
0.5	0.1	0.5	1.0	0.1	0.1	−0.140078	0.023735	1.247951	0.916867
0.5	0.4	0.5	1.0	0.1	0.1	−0.250201	0.031057	1.352539	0.955381
0.5	0.7	0.5	1.0	0.1	0.1	−0.380552	0.038807	1.464718	0.994421
0.5	1.0	0.5	1.0	0.1	0.1	−0.587237	0.049129	1.626014	1.048395
0.5	1.5	0.5	1.0	0.1	0.1	−0.831464	0.058702	1.800411	1.106039
0.5	0.5	0.1	1.0	0.1	0.1	−0.125666	0.022952	1.126172	1.004751
0.5	0.5	0.3	1.0	0.1	0.1	−0.106883	0.022122	0.985623	1.109165
0.5	0.5	0.5	1.0	0.1	0.1	−0.101728	0.021884	0.949521	1.135298
0.5	0.5	0.7	1.0	0.1	0.1	−0.092453	0.021452	0.888128	1.179056
0.5	0.5	1.0	1.0	0.1	0.1	−0.080692	0.020910	0.815602	1.229572
0.5	0.5	0.5	0.1	0.1	0.1	0.232941	0.026897	1.131447	1.473229
0.5	0.5	0.5	0.6	0.1	0.1	0.189636	0.025347	1.164016	1.250944
0.5	0.5	0.5	1.1	0.1	0.1	0.145116	0.023823	1.198808	1.008882
0.5	0.5	0.5	1.5	0.1	0.1	0.099296	0.022319	1.236250	0.743977
0.5	0.5	0.5	2.0	0.1	0.1	0.039967	0.020474	1.287598	0.374770
0.5	0.5	0.5	1.0	0.1	0.1	0.142382	0.023843	1.265463	0.903797
0.5	0.5	0.5	1.0	0.3	0.1	0.133788	0.023442	1.207902	0.944932
0.5	0.5	0.5	1.0	0.5	0.1	0.124237	0.023009	1.135199	0.998566
0.5	0.5	0.5	1.0	0.7	0.1	0.114095	0.022566	1.043630	1.068728
0.5	0.5	0.5	1.0	1.0	0.1	0.110503	0.022566	1.043630	1.068728
0.5	0.5	0.5	1.0	0.1	0.1	0.133788	0.023442	1.207902	0.944932
0.5	0.5	0.5	1.0	0.1	0.3	0.163289	0.065066	1.208374	0.945285
0.5	0.5	0.5	1.0	0.1	0.5	0.185200	0.101119	1.208910	0.945701
0.5	0.5	0.5	1.0	0.1	0.7	0.201958	0.132848	1.209486	0.946153

Graphs:

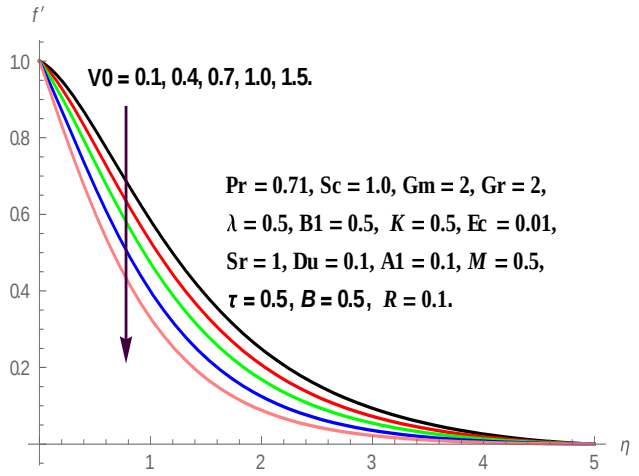

Figure 2. Effect of (V_0) on Velocity profiles.

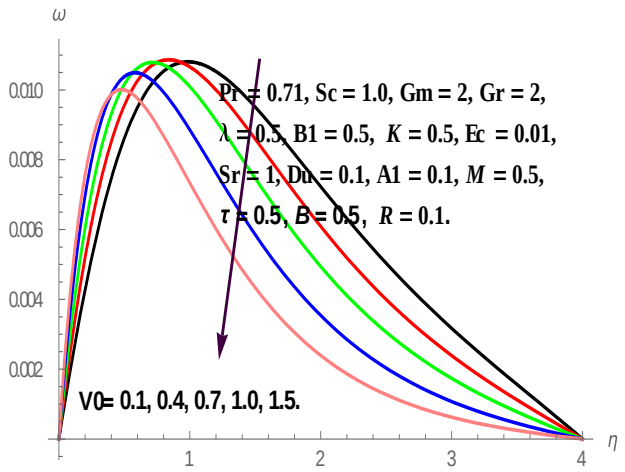

Figure 3. Effect of (V_0) on angular velocity profiles.

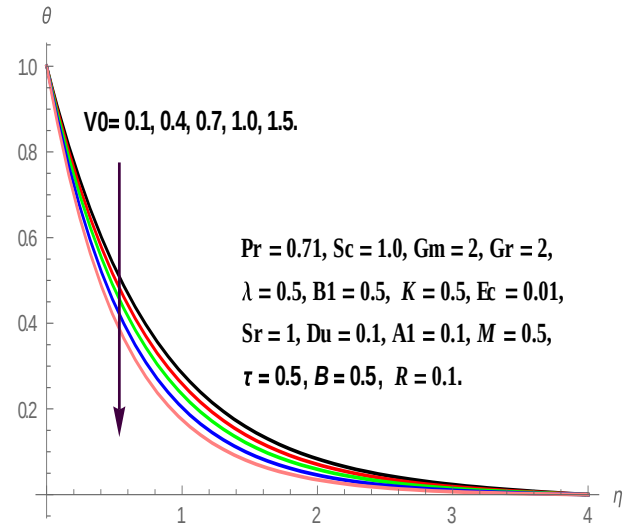

Figure 4. Effect of (V_0) on Temperature profiles.

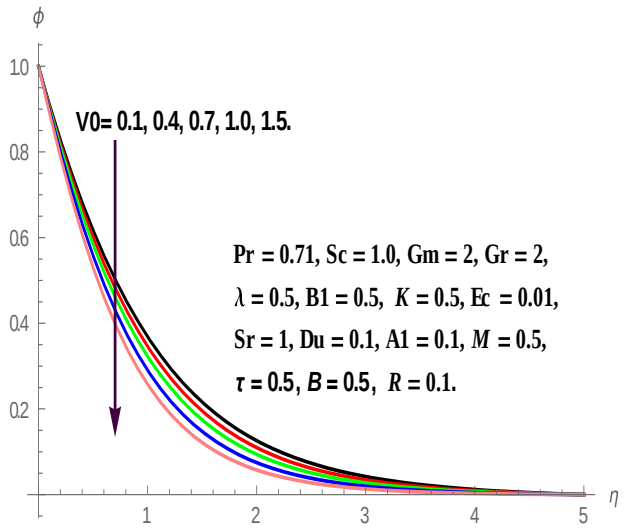

Figure 5. Effect of (V_0) on Concentration profiles.

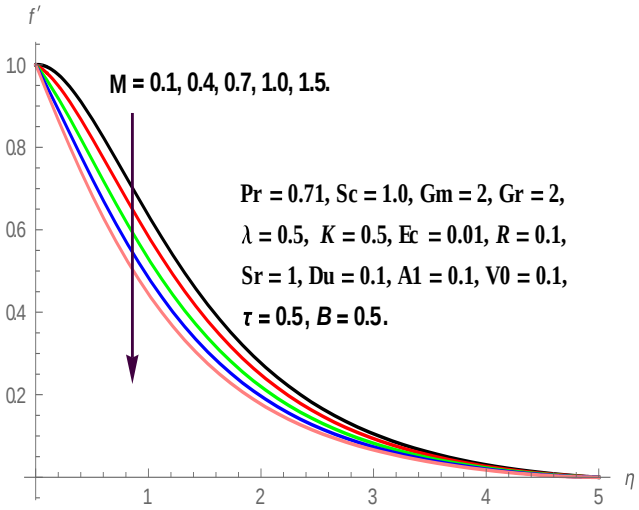

Figure 6. Effect of (M) on Velocity profiles.

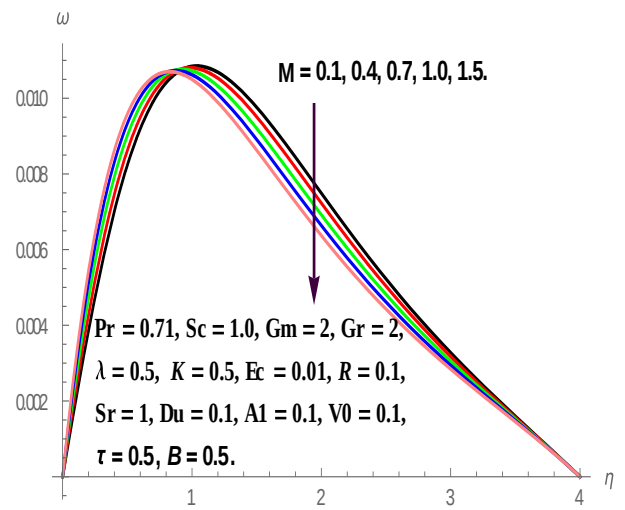

Figure 7. Effect of (M) on angular velocity profiles.

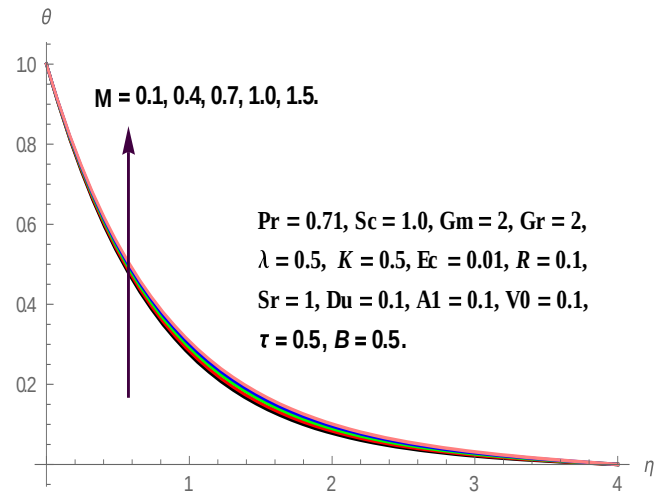

Figure 8. Effect of (M) on Temperature profiles.

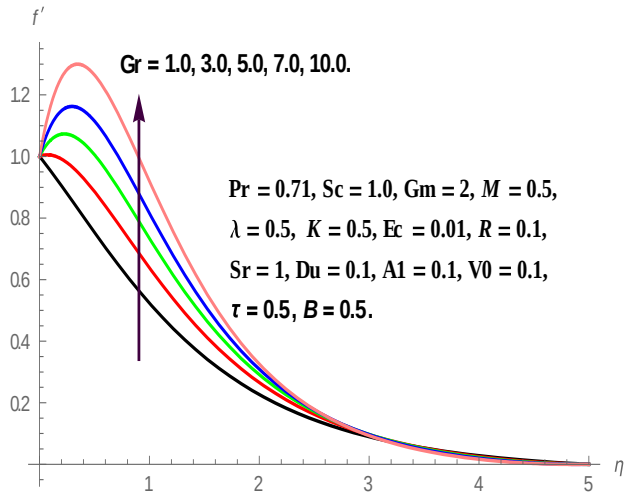

Figure 9. Effect of (Gr) on velocity profiles.

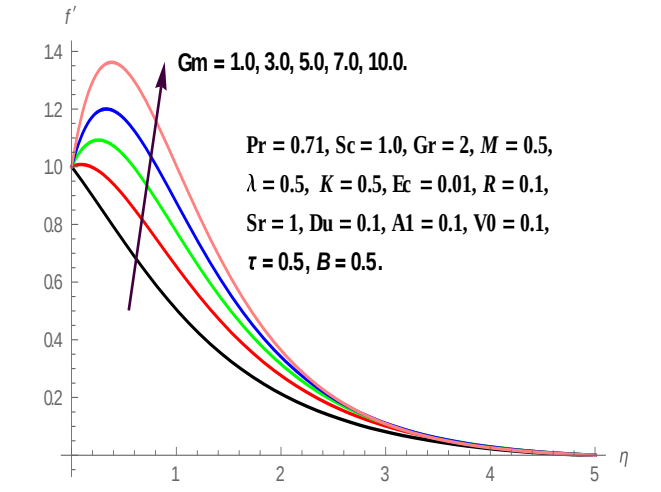

Figure 10. Effect of (Gm) on Velocity profiles.

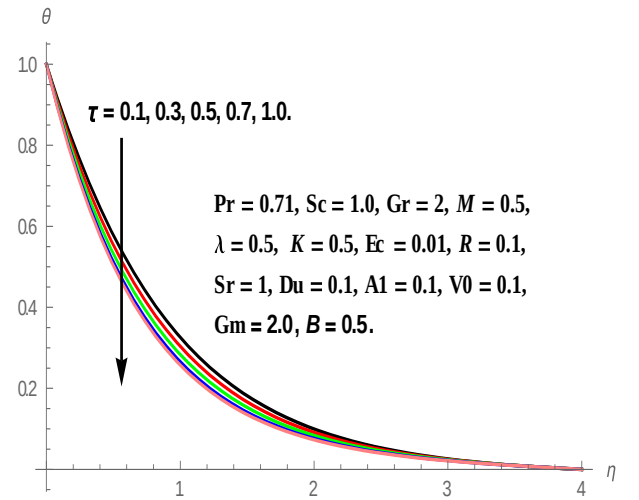

Figure 11. Effect of (τ) on Temperature profiles.

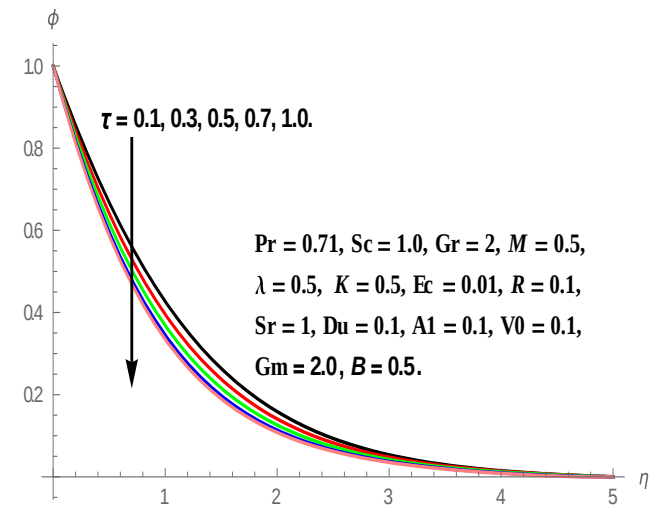

Figure 12. Effect of (τ) on Concentration profiles.

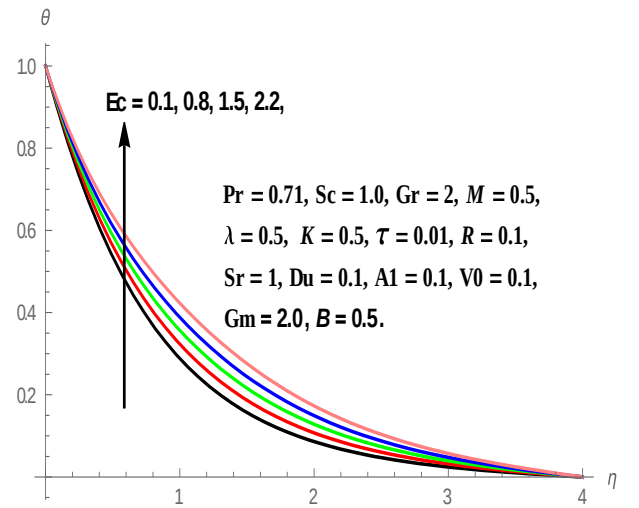

Figure 13. Effect of (Ec) on Temperature profiles.

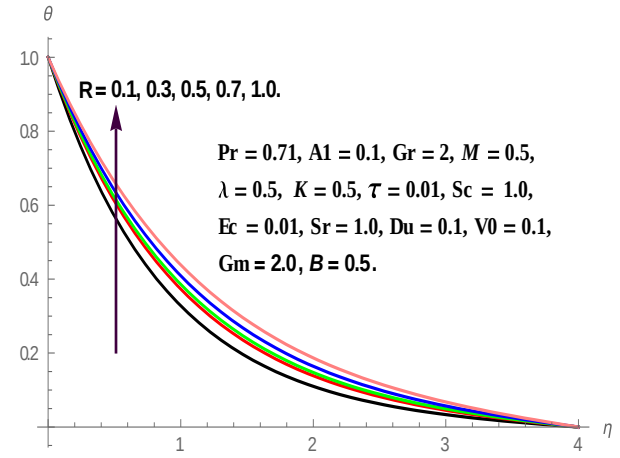

Figure 14. Effect of (R) on Temperature profiles.

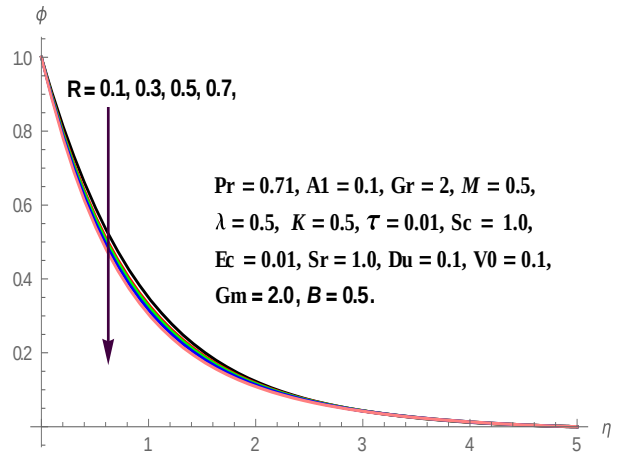

Figure 15. Effect of (R) on Concentration profiles.

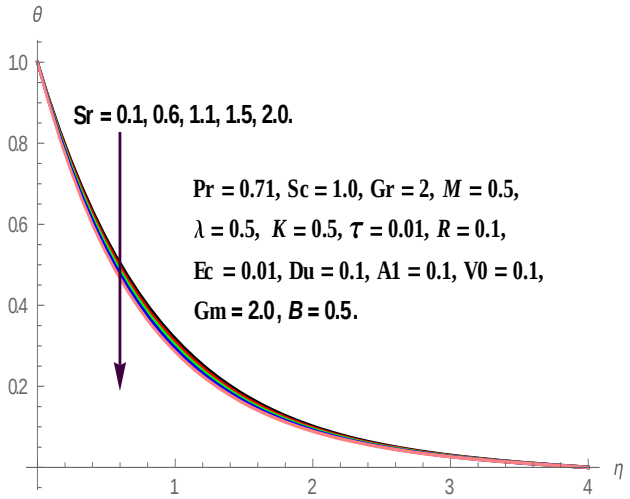

Figure 16. Effect of (Sr) on Temperature profiles.

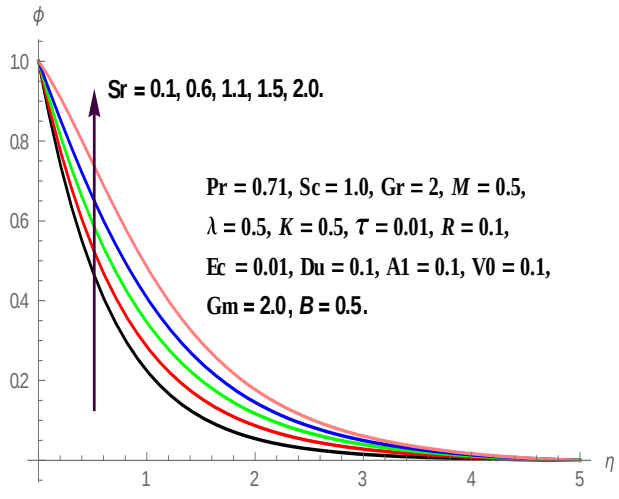

Figure 17. Effect of (Sr) on Concentration profiles.

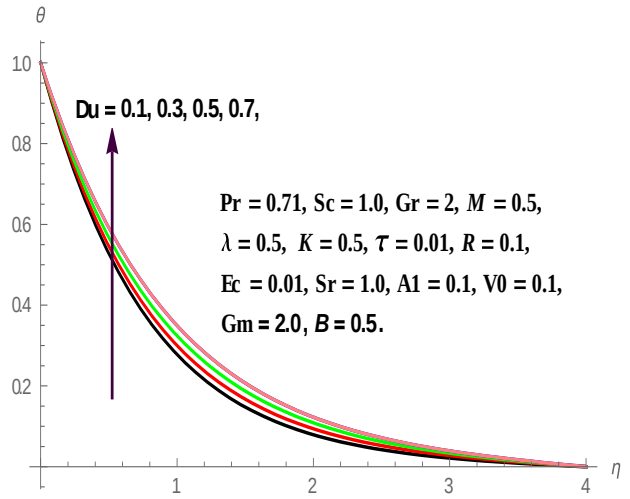

Figure 18. Effect of (Du) on Temperature profiles.

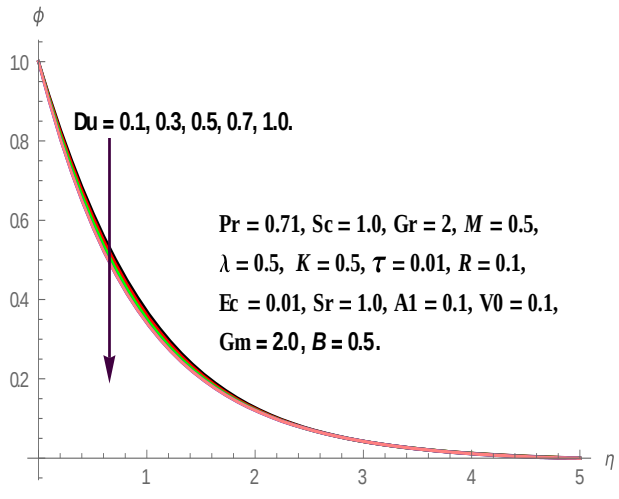

Figure 19. Effect of (Du) on Concentration profiles.

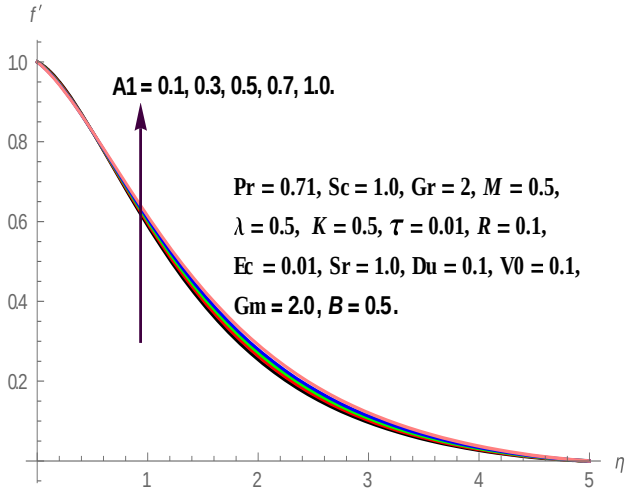

Figure 20. Effect of ($A1$) on Velocity profiles.

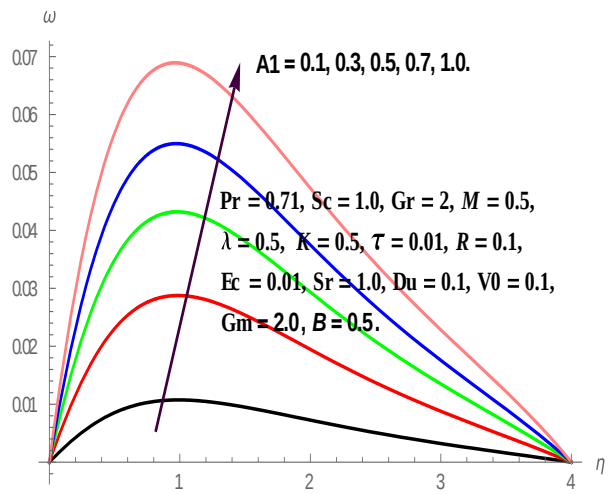

Figure 21. Effect of ($A1$) on angular velocity profiles.